Helicity of Solar Active-Region Magnetic Fields

Richard C. Canfield and Alexei A. Pevtsov
Physics Department, Montana State University
Bozeman, MT 59717-3840, U.S.A.

Abstract.
We briefly discuss the concept of magnetic helicity and the formalism for thin magnetic flux tubes. We describe photospheric active-region observations to which it is relevant, emphasizing vector magnetograms. We review discoveries about the helicity of magnetic fields in the photosphere and corona made using synoptic vector magnetograms from the Haleakala Stokes Polarimeter (HSP) at Mees Solar Observatory, in combination with the Yohkoh Soft X-ray Telescope (SXT): the hemispheric rule for handedness (chirality), the subphotospheric origin of coronal currents, large-scale long-lived patterns of handedness, the relationship between twist and tilt in active regions, and the role of helicity in trans-equatorial coronal reconnection. We close by discussing our interpretation of these observations and the importance of improved synoptic vector magnetograms.

1. Introduction

Synoptic observations of active regions in the solar atmosphere have much to teach us about conditions in and below the convection zone. Howard (1996) has recently reviewed how the physical conditions in subsurface layers of the Sun and the nature of magnetic flux bundles that form active regions are reflected in the structure and behavior of these regions at the surface. The key synoptic observations for these studies have been those made at Mount Wilson observatory, and include longitudinal magnetic field measurements and daily white-light photographs.

The last two decades have seen the quality of observations with photospheric vector magnetographs develop to a level of quantitative significance. The observation of the full magnetic vector, not just its line-of-sight component, adds a significant new dimension. Vector magnetographs commonly show twist in active-region magnetic fields. Although photospheric magnetic fields are not plausibly force-free, the value of the force-free field parameter α ($\nabla \times \mathbf{B} = \alpha\mathbf{B}$) that best fits the fields observed in the vector magnetograms is a convenient way of characterizing that twist. Results from such observations are emphasized in this review.

The reader fully hooked on helicity is referred to Rust (1997) and others in the same publication for reviews of results derived from complementary coronal, interplanetary and morphological techniques. Observations of the coronal structure of solar active regions with the Yohkoh Soft X-ray Telescope (Tsuneta 1991) commonly show S and inverse-S structures (Acton *et al.* 1992), which show a hemispheric preference (Rust & Kumar 1996). The southern hemisphere is conveniently marked with S structures. The inverse-S structures which predominate in the North, aligned as they are along parallels of latitude, even tend to look like N's! In any case, such structures can be modeled from photospheric vector magnetograms, allowing us to relate what we see in the corona to the large-scale photospheric magnetic fields of these regions. These coronal structures give us fascinating insight into the role of helicity and currents in reconnection.

2. Helicity of Magnetic Flux Tubes

Consider a magnetic field $\mathbf{B}(\mathbf{x}) = \nabla \times \mathbf{A}(\mathbf{x})$ in a domain $\mathcal{D}$ on whose surface $\mathbf{n} \cdot \mathbf{B} = \mathbf{0}$. The magnetic helicity $\mathcal{H}$ of this flux system is then $\mathcal{H} = \int_{\mathcal{D}} \mathbf{A} \cdot \mathbf{B}\ \mathrm{dV}$. Consider a thin tube T with local $\mathbf{B}(\mathrm{r}, \theta, \mathrm{z})$ defined by its axial component $\mathbf{B}_{\mathrm{a}} = (0, 0, \mathrm{B_z(r)})$ and meridional component $\mathbf{B}_{\mathrm{m}} = (0, \mathrm{B}_\theta(\mathrm{r}), 0)$. Moffatt & Ricca (1992) showed that the total magnetic helicity $\mathcal{H}$ is given by $\mathcal{H} = \int_{\mathrm{T}} \mathbf{A}_{\mathrm{a}} \cdot \mathbf{B}_{\mathrm{a}}\ \mathrm{dV} + 2\int_{\mathrm{T}} \mathbf{A}_{\mathrm{m}} \cdot \mathbf{B}_{\mathrm{m}}\ \mathrm{dV}$. The axial term gives the *writhe* contribution $\mathcal{W} = \int_{\mathrm{T}} \mathbf{A}_{\mathrm{a}} \cdot \mathbf{B}_{\mathrm{a}}\ \mathrm{dV}$, and the meridional term gives the *twist* contribution $\mathcal{T} = 2\int_{\mathrm{T}} \mathbf{A}_{\mathrm{m}} \cdot \mathbf{B}_{\mathrm{m}}\ \mathrm{dV}$, where $\mathbf{B}_{\mathrm{a}} = \nabla \times \mathbf{A}_{\mathrm{a}}$ and $\mathbf{B}_{\mathrm{m}} = \nabla \times \mathbf{A}_{\mathrm{m}}$.

We *cannot* observe a full flux system $\mathcal{D}$ of an active region, since it extends below the visible surface, so we cannot observationally determine $\mathcal{H}$, $\mathcal{W}$, or $\mathcal{T}$. We *can* measure local values of quantities that contribute to the integrand $\mathbf{A} \cdot \mathbf{B}$. Using vector magnetograms, we determine the photospheric vertical current density j_z over a horizontal area S: $j_z = (\mu_0 S)^{-1} \oint \mathbf{B} \cdot d\ell = \boldsymbol{\mu_0}^{\mathbf{-1}}\ \nabla \times \mathbf{B}$. For a force–free field $(\nabla \times \mathbf{B})_z = (\alpha \mathbf{B})_z = \mu_0 j_z$. For a linear (constant–α) force–free field $\mathbf{A} \cdot \mathbf{B} = \alpha^{-1} \mathbf{B}^2$. We use the force–free field parameter α to describe our data, since it can be derived from observations whether $\mathbf{B}$ is force free or not, and it is a local measure of the integrand of $\mathcal{H}$ if $\mathbf{B}$ is force–free, as in the Sun's corona.

The sign of α is a measure of the handedness (chirality) of the field; $\alpha > 0$ for right-handed fields. The magnetic helicity $\mathcal{H}$ is a conserved quantity in ideal MHD, and nearly so in at least some circumstances relevant to the Sun, which we will not elaborate here. On the other hand, the current helicity $\mathbf{B} \cdot \nabla \times \mathbf{B}$ (related to the force-free field parameter α), an analogue to the kinetic helicity $\mathbf{v} \cdot \nabla \times \mathbf{v}$ of flows, is a local quantity, and is not conserved.

3. The Haleakala Stokes Polarimeter Dataset

The vector magnetogram dataset from which the reviewed research is drawn consists of about 1000 vector magnetograms of a few hundred active regions obtained with the Haleakala Stokes Polarimeter (Mickey 1985) at Mees Solar Observatory in 1988 - 1996. This instrument provides simultaneous Stokes I, Q, U, and V profiles of the Fe I $\lambda\lambda$6301.5, 6302.5 Å doublet (Landé g factor $g_L = 1.67, 2.5$) at ≈ 25 mÅ/pixel dispersion. Magnetograms are obtained by a rectangular raster scan. A typical scan is $2' \times 2'$ or larger, has a pixel spacing of $2.''8$ ("high-resolution scan") or $5.''6$ ("low-resolution scan"), integrates each measurement for 2 s or 3.5 s respectively, and takes an hour or so to complete.

Light enters the analysis section of the polarimeter through a 6″ pinhole, so a pixel spacing $\leq 3''$ yields critically sampled data at a true resolution of 6″.

At each raster point the strength of the magnetic field parallel and transverse to the line of sight, and the azimuth ϕ of the transverse field, are determined by one of two methods depending on the fractional polarization. When the polarization is $\geq 1\%$ (corresponding to a field strength $\gtrsim 100$ G) we perform a nonlinear least-squares fit of theoretical Stokes profiles to both Fe I lines (Skumanich & Lites 1987). The advantage of this method is its ability to avoid false helicity signals due to magneto-optical effects and to make first-order corrections for incomplete spatial resolution. In low-field regions the field is determined using integrated properties of the Stokes profiles (Ronan, Mickey, & Orrall 1987). The angle ϕ is ambiguous by 180°. We resolve this ambiguity using a multi-step process described in detail in the appendix of Canfield *et al.* (1993).

The ambiguity-resolved vector magnetogram is transformed to disk-center heliographic coordinates, thus eliminating projection effects. From the heliographic vector magnetogram we then derive the vertical current density j_z using Ampère's Law,

$$\frac{4\pi}{c} j_z = (\nabla \times \mathbf{B}) \cdot \hat{\mathbf{z}} = \frac{\partial \mathbf{B_y}}{\partial \mathbf{x}} - \frac{\partial \mathbf{B_x}}{\partial \mathbf{y}}.$$

The derivatives are approximated by a four-point differencing scheme; the current is therefore computed at each intersection of four magnetogram pixels. We perform no additional filtering or smoothing of the data.

Maps of $\alpha = \mu_0 \; j_z/B_z$ are then created from the maps of the vertical current density. Such maps typically show significant variation of α within an individual active region, both in magnitude and sign (Pevtsov, Canfield, and Metcalf 1994). However, there is often a pronounced overall twist to an active region. To characterize this overall twist we determine α_{best}, the single value of α for a linear force-free field that best fits the observed vector fields at all points in the magnetogram, in a least-squares sense.

4. Hemispheric Variation of Twist

The handedness of the twisted fields of active regions observed in the photosphere shows a hemispheric difference at the 2 σ level, as shown in Figure 1. An earlier version of this figure, based on far fewer active regions, was published by Pevtsov, Canfield, and Metcalf (1995). Figure 1 shows the results for the full HSP dataset, in which 76% of the active regions in the northern hemisphere have negative α (left handedness), and 69% in the southern hemisphere, positive.

A strength of magnetograph measurement of α in the photosphere, in contrast to the measurement of angles within S and inverse-S structures in the corona, is its more quantitative nature, which accrues from lesser sensitivity to projection effects. It has to be noted, however, that this method is presently limited to the strong fields of active regions, a limitation that does not apply to methods that use coronal morphology.

Bearing this point in mind, it is interesting to note that although the HSP data show considerable variation from one active region to the next, the dataset as a whole also reveals that the magnitude of the average value of α_{best} depends on latitude, starting near zero at the equator, reaching a maximum near 15–20

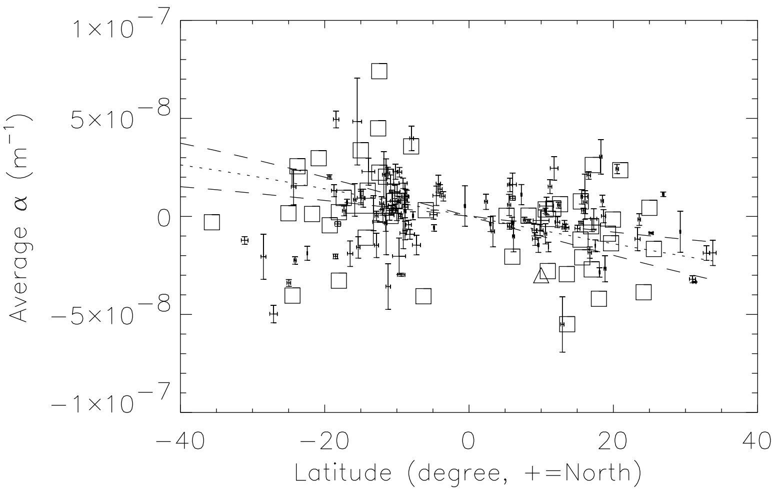

Figure 1. Observed latitude dependence of large-scale twist (measured by the average value of α_{best}) of active regions in the HSP dataset. The error bars show one standard deviation of both α and latitude. Box symbols without error bars show α of active regions represented by only one magnetogram. The short-dashed line shows the least-squares best linear fit and the dashed lines show the 95% confidence band.

degrees in both hemispheres, and dropping back above 35–40 degrees. Such latitudinal variation may result from turbulent convective motions, the Coriolis force, and differential rotation.

5. Subhotospheric Origin of Coronal Currents

Using photospheric vector magnetograms from the HSP dataset and coronal X-ray images from SXT, Pevtsov, Canfield, & McClymont (1997) inferred values of the force-free field parameter α at both photospheric and coronal levels within 140 active regions from the HSP dataset, for which suitable Yohkoh data were available. We determined α_{best} for each magnetogram, then averaged the α_{best} values from all available magnetograms to obtain a single mean photospheric α value $< \alpha_p >$ for each active region.

S and inverse-S structures like those highlighted in the central force-free field lines of a simple bipole, shown in Figure 2, abound in the corona. Using clearly formed S and inverse-S structures observed with SXT, we estimated α in the corona by determining (π/L) sin γ for individual loops, where γ is the observed angle at which X-ray loops of length L cross the axis of the active region. We then averaged these values to obtain a single coronal α value, $< \alpha_c >$, for each active region.

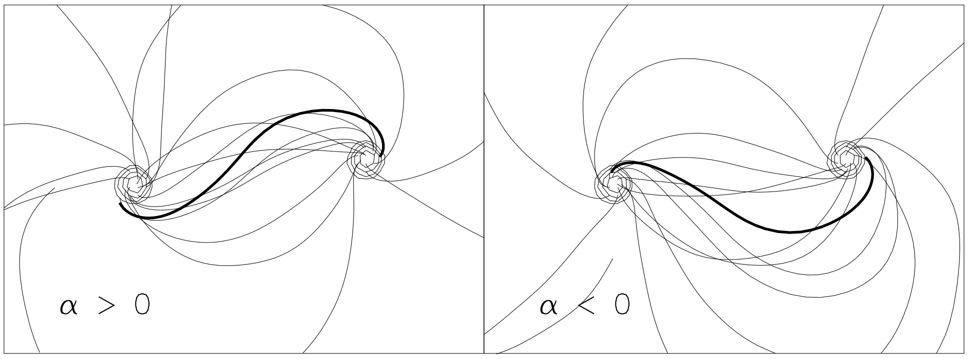

Figure 2. Model bipolar linear force-free fields computed for positive and negative α. Contours show vertical magnetic field strength. Magnetic field lines are projected onto the horizontal plane. A low-lying field line near the central part of the dipole is shown in bold, to demonstrate the sense of shear (*i.e.*, S for positive α and inverse-S for negative α).

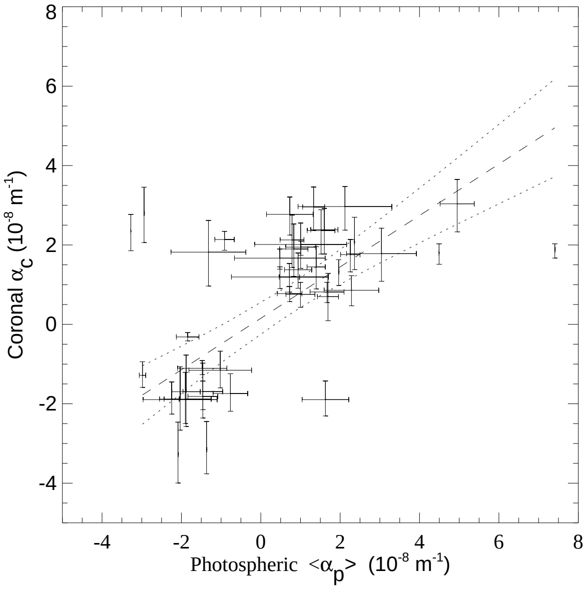

Figure 3. Observed force-free field parameter α from photospheric vector magnetograms ($< \alpha_p >$) and from the shape of coronal loops ($< \alpha_c >$) for 44 active regions. Error bars show one standard deviations in both parameters. Error bars for coronal $< \alpha_c >$ correspond to 10° standard deviation in shear. Active regions without error bars in $< \alpha_p >$ are represented by only one magnetogram. The linear fit (long dashed line) and 2 σ error band (short dashed lines) are shown.

In the 44 active regions whose photospheric α map is predominantly of one sign, we found that the values of $< \alpha_p >$ and $< \alpha_c >$ are correlated, as shown in Figure 3. In the remaining regions, localized regions show large variations in α values, and both signs of α are well represented. For them, our analysis method breaks down, and the values of $< \alpha_p >$ and $< \alpha_c >$ poorly correlated (not shown). The former correlation implies that coronal electric currents typically extend down to at least the photosphere. Other studies, discussed below, imply that the currents that are observed in the photosphere originate far deeper (see also Leka *et al.* 1996, McClymont, Jiao & Mikic 1997). We therefore believe that the currents responsible for sinuous coronal structures in active regions originate deep within the convection zone or at the shear zone at its base.

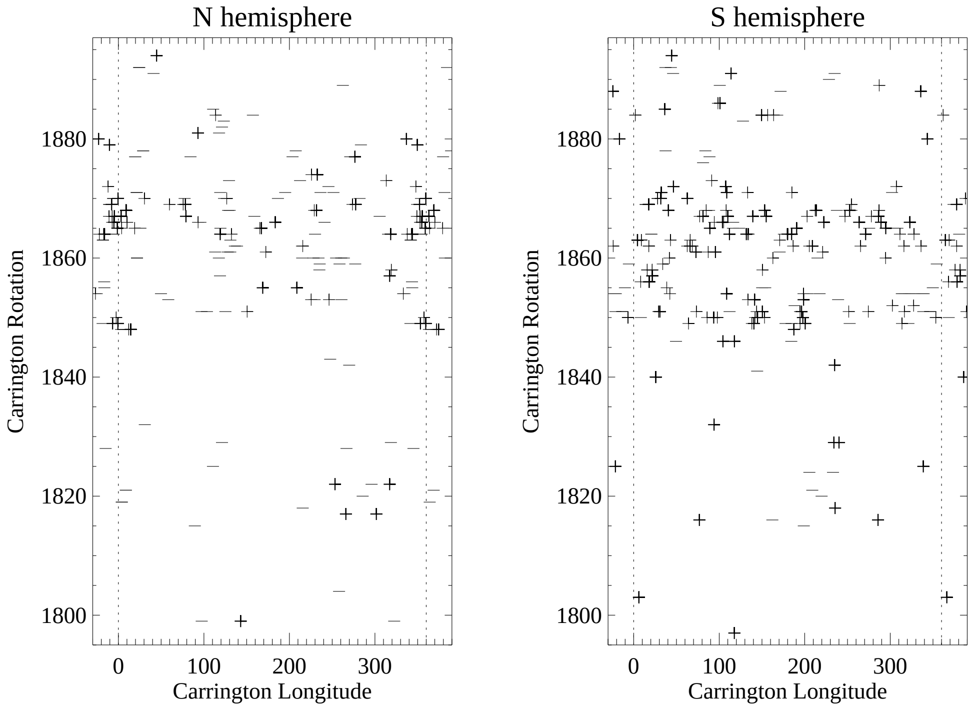

Figure 4. Carrington longitude–rotation charts for the northern (left) and southern (right) hemispheres. The + and − symbols indicate the sign of α (*i.e.*, the handedness or chirality) for the active region. Both HSP vector magnetograms and SXT images were used to build this figure.

6. Large-Scale Long-Lived Patterns

The convection-zone distribution of kinetic helicity is important to the solar dynamo. Although direct measurements are impossible, kinetic helicity may be studied through observations of the helicity of photospheric fields. If the Coriolis force plays a role, the chirality of magnetic fields should change between hemispheres. The hemispheric rule, however, is rather weak, *i.e.* many active regions show handedness which does not conform to the rule. It is interesting that Figure 4 shows areas that keep the same sign of α for many rotations, including some that disagree with the hemispheric rule. The best example of such an area is seen in the northern hemisphere near 360° between solar rotations 1862–1870. Such areas may be the result of large–scale motions in the convective zone. Support for this view comes from the persistence of these areas for several successive rotations, implying that the helicity of the fields in these regions has been generated at great depths, not near to the surface. For these rather basic reasons, we believe that long-lived large-scale organization of convection exists in the region where the helicity is created.

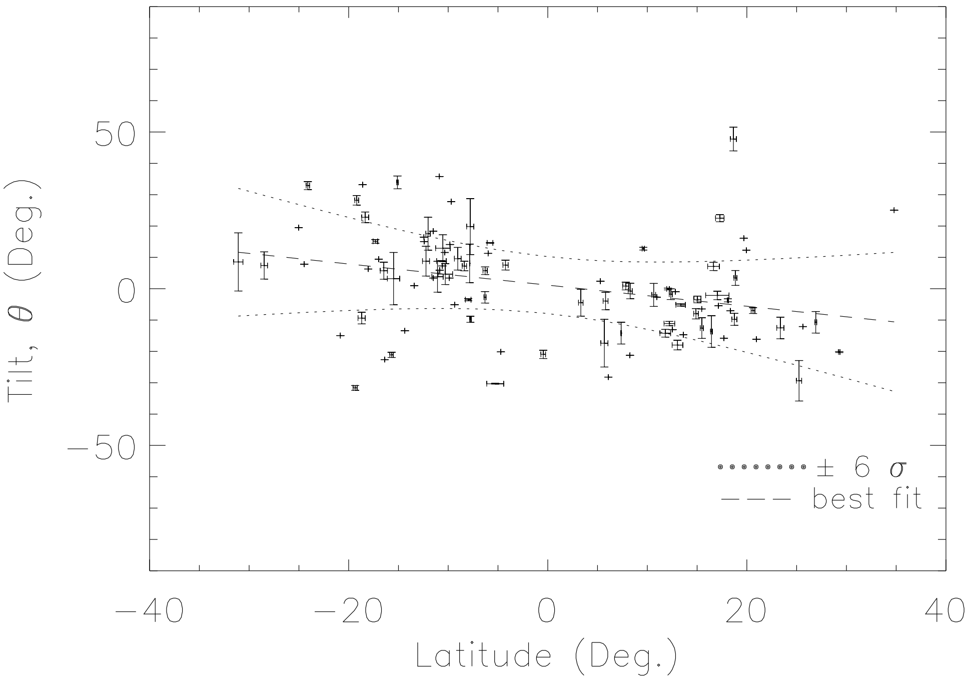

Figure 5. The dependence of the active region tilt on latitude for all 99 active regions. Error bars are given when there is more than one magnetogram per region. The long-dashed line shows the best least-squares fit. The short-dashed lines define the $\pm$ 6σ error band of the fit.

7. Twist and Tilt of Active Regions

Pevtsov & Canfield (1998) used a subset of the HSP dataset (about 300 magnetograms of 99 active regions) for which we could determine both θ, the tilt of the active region axis with respect to the solar equator (positive in the counter-clockwise direction) and L, the separation of the centroid of the N and S polarities, as well as α_{best} and λ, the helio-latitude of the active region. We eliminated from this subset eight regions that disobeyed the Hale & Nicholson (1938) polarity law, because they might be due to kinked Ω loops, for which θ is ambiguous.

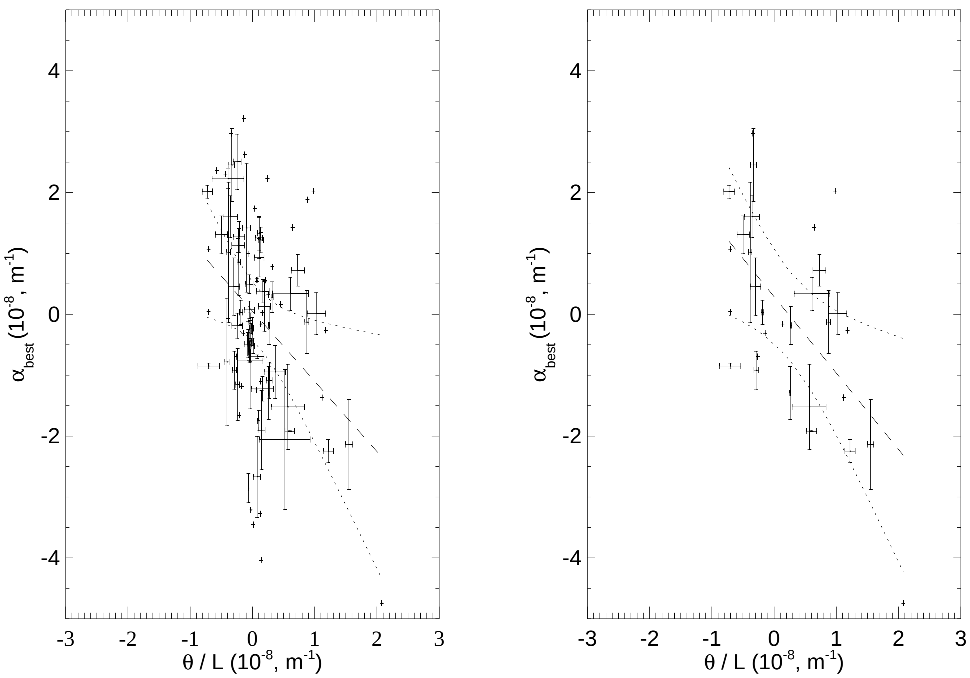

Figure 6. The dependence of observed active region α_{best} on the ratio of tilt to characteristic length. Left: All 91 regions that obey the Hale-Nicholson polarity law. Right: Only those regions that depart from Joy's law by more than $\pm$ 6σ (see Fig. 1). The long-dashed lines are linear least-squares fits; the short-dashed curves define the $\pm$ 3σ error bands.

Consider a simple model in which, at the base of the convection zone, flux tubes are simple axisymmetric toroids, without intrinsic twist. When they rise through the convection zone the Coriolis force on the flow in the rising tube produces right-handed writhe ($\mathcal{W} > 0$, corresponding to $\theta < 0$) in the Northern hemisphere. From helicity conservation, we then expect the production of left-handed twist ($\mathcal{T} < 0$, corresponding to $\alpha < 0$) in the Northern Hemisphere. We also then expect $\alpha < 0$ ($\mathcal{T} < 0$) when $\theta < 0$ ($\mathcal{W} > 0$).

Active regions show a hemispheric relationship in the tilt of active regions with respect to the solar equator, called Joy's law (Hale *et al.* 1919). This hemispheric relationship, in our dataset, is shown in Figure 5. The simple model therefore leads us to expect a hemispheric dependence of twist, with $\alpha < 0$ in the Northern hemisphere because of helicity conservation and $\mathcal{W} > 0$ ($\theta < 0$) there. Observations of active region α values show such a relationship (Seehafer 1990, Pevtsov, Canfield, and Metcalf 1995), as discussed above.

The relationship between α_{best} and tilt (per unit length) for those regions is shown in Figure 6, for two datasets. On the left, all 91 regions that obey the Hale-Nicholson law are plotted. On the right, only those of these regions that depart by more than $\pm$ 6σ from Joy's law are shown. In both, the slope of the relationship between α_{best} and θ/L is essentially -1. The relationship is opposite that of the simple model introduced above. We therefore believe that

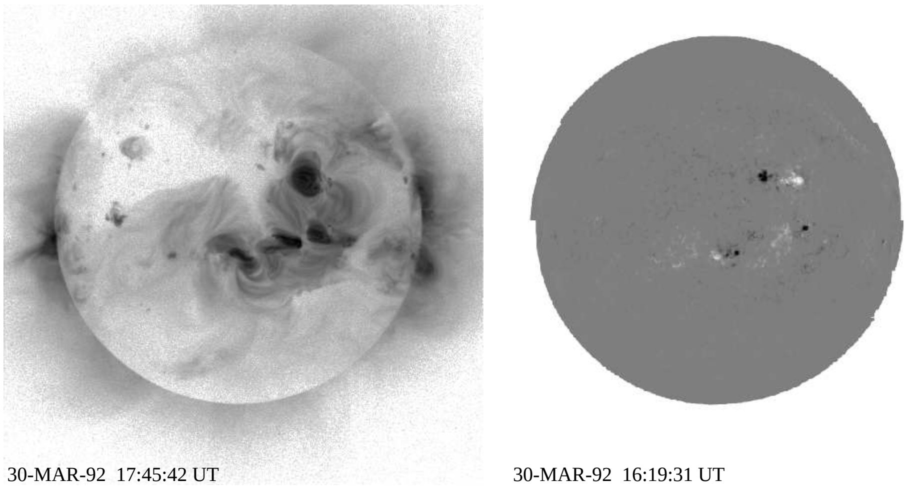

Figure 7. SXT image (negative) and Kitt Peak magnetogram (white indicates negative magnetic field) showing a well-connected trans-equatorial pair of regions of the same (negative) chirality, AR 7116 ($\sim$S05W15) and AR 7117 ($\sim$N06W15).

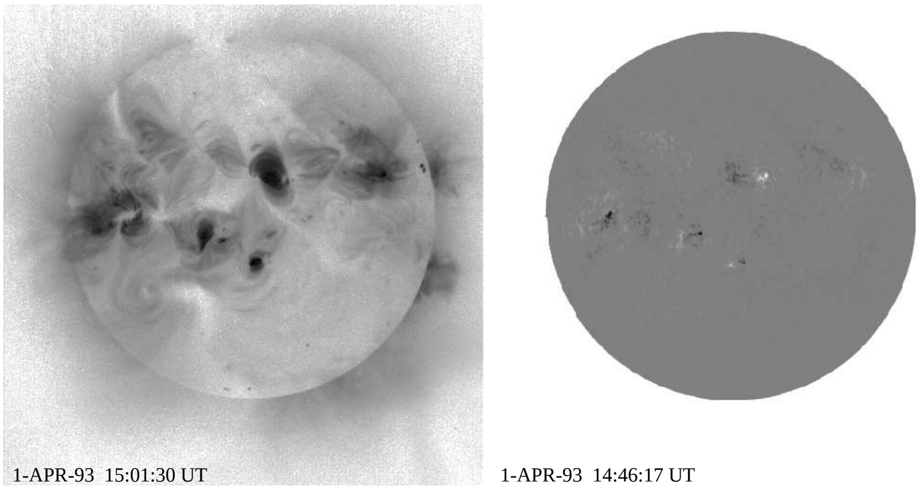

Figure 8. SXT image (negative) and Kitt Peak magnetogram showing three regions that are close in longitude, but are not well connected across the equator. NOAA AR 7461 ($\sim$N04W04) has negative chirality, but NOAA AR 7463 ($\sim$S07E09) and NOAA AR 7466 ($\sim$S14W01) have positive chirality.

the twist observed in active region magnetic fields is not the consequence of flows that occur along them during their rise through the convection zone.

8. Trans-equatorial Reconnection

Trans-equatorial reconnection is interesting in the framework of the dynamo and the transport of helicity from the Sun. Canfield, Pevtsov, & McClymont (1996) used the HSP and SXT datasets to study the role of helicity in the trans-equatorial reconnection of active regions. They identified 27 pairs of regions reasonably close to one another in opposite hemispheres, which had both HSP magnetograms and detectable S or inverse-S structure. They compared cases in which regions connected very well across the equator (Figure 7) to those in which regions connected very poorly. They found that active regions reconnect preferentially with others of the same chirality. They explained this result with a simple model of the closure of their current systems; only when the chirality of the regions is the same on opposite sides of the equator can both flux closure and current closure be achieved through reconnection without altering the magnetic flux and current density distribution at photospheric levels (see also Melrose 1997).

9. Interpretation

The synoptic vector magnetograph observations reviewed above lead to the following interpretations:

- The Coriolis force and large-scale convection zone flows play at least some role in the generation of twist in active-region magnetic fields. The temporal and spatial scales of long-lived global patterns of active-region twist suggest that they are created by large-scale convection-zone flows. Even though the hemispheric handedness rule is weak, it is not negligible, and the trans-equatorial change of sign of the handedness of the observed active region fields suggests the Coriolis force. On the other hand, the weakness of the hemispheric chirality rule and Joys' law suggests that turbulence is also important to the generation of twist and writhe.

- The twist of active region magnetic fields observed in both the photosphere and the corona originates beneath the visible surface. Bearing in mind the discovery of large-scale long-lived twist patterns, we conclude that the twist observed in the photosphere must originate either well within the convection zone or at its base, and not at the photosphere/corona interface.

- The observed twist of active region magnetic fields is not the consequence of flows within Ω loops as they rise through the convection zone. The Coriolis force on rising Ω loops fails to explain the observed twist/writhe relationship.

- Helicity and current closure play a role in coronal reconnection (see also Pevtsov, Canfield, & Zirin 1996, Melrose 1997, Canfield & Reardon 1998 for its relevance to flares).

10. Open Questions

The theory of magnetic helicity is rich, and the concept has proven valuable in the study of laboratory and space plasmas. We have good reason to expect it to be useful in solar physics, as well. The use of the HSP vector magnetograph observations to better understand the solar physics implied by helicity observations is presently limited by low duty cycle, low spatial resolution (and consequent low magnetic sensitivity), and bias toward flare-productive active regions. Many fundamental questions remain open:

- How do patterns of helicity inside active regions reflect solar interior conditions? What is the lifetime and latitude dependence of patterns as a function of scale size? Do episodes of repeated emergence and submergence take place? Is there evidence for relaxation of the patterns?
- What is the origin of the hemispheric rule? What is the latitude dependence of α in an unbiased sample of active regions? How does the lifetime and structure of regions depend on their conformity to the hemispheric rule? Are regions that do not obey the hemispheric rule more flare productive? What is the solar-cycle dependence of nests of exceptional regions?
- How can the relationship between twist and writhe be understood? Is the presently-understood relationship quantitatively robust, or is higher spatial resolution important? What is the evidence for, and origin of, kinks in Ω loops?
- What is the role of helicity transfer by reconnection in the solar dynamo, in eruptive flares and CMEs, in emerging flux, jets and surges?
- What is the role of helicity conservation and current closure in reconnection? How do they play a role in eruptive flares, coronal mass ejections, trans-equatorial reconnection, and the solar dynamo?

We look forward to the day when these fundamental questions can be addressed with synoptic full-disk vector magnetograph observations with superior resolution and sensitivity, unimpeded by the day/night cycle.

Acknowledgments. We thank Don Mickey for his key role in developing the Haleakala Stokes Polarimeter, and the Mees staff for maintaining and operating it for many years. We thank Tom Metcalf and Sandy McClymont for their collaboration, Dana Longcope, Isaac Klapper, and Fausto Cattaneo for discussions, and Nariaki Nitta for comments on the manuscript. This research has been supported by NASA, through Supporting Research and Technology Grants NAGW-5072 and NAG5-5043 and the Yohkoh Soft X-ray Telescope contract NAS8-40801.

References

Acton, L. W., *et al.* 1992, Science, 258, 618

Canfield, R. C., *et al.* 1993, ApJ, 411, 362.

Canfield, R. C., & Reardon, K. P. 1998, Sol. Phys., submitted.

Canfield, R. C., Pevtsov, A. A., & McClymont, A. N. 1996, in Magnetic Reconnection, ed. R. Bentley & J. Mariska, A.S.P. Conf. Series, 111, 341 (1996)

Hale, G. E., & Nicholson, S. B., 1938, Carnegie Inst. Wash. Publ., 49, 8.

Hale, G. E., Ellerman, F., Nicholson, S. B., & Joy, A. H. 1919, ApJ, 49, 153.

Howard, R. F. 1996, Annu. Rev. Astron. Astrophys. 34, 75.

Leka, K. D., Canfield, R. C., McClymont, A. N., & van Driel-Gesztelyi, L. 1996, ApJ, 462, 547.

Longcope, D. W. & Klapper, I. 1997, ApJ, 488, in press.

McClymont, A. N., Jiao, L., & Mikic, Z. 1997, Sol. Phys., in press.

Melrose, D. B., 1997, ApJ, 486, 521.

Mickey, D. L., 1985, Sol. Phys., 97, 223.

Moffatt, H.K., & Ricca, R.L., 1992, Proc. R. Soc. Lond. A, 439, 411.

Pevtsov, A. A., & Canfield, R. C. 1998, ApJ (submitted).

Pevtsov, A. A., Canfield, R. C., & McClymont, A. N. 1997, ApJ, 481, 973.

Pevtsov, A. A., Canfield, R. C., & Metcalf, T. R. 1994, ApJ, 425, L117.

Pevtsov, A. A., Canfield, R. C., & Metcalf, T. R. 1995, ApJ, 440, L109.

Pevtsov, A. A., Canfield, R. C., & Zirin, H. 1996, ApJ, 473, 533.

Ronan, R. S., Mickey, D. L., & Orrall, F. Q. 1987, Sol. Phys., 113, 353.

Rust, D. M., 1997, in Coronal Mass Ejectons, ed. N. Crooker, J. A. Joselyn, & J. Feynman, AGU Geophysical Monograph 99, 119.

Rust, D. M., & Kumar, A. 1996, ApJ, 464, L199.

Seehafer, N., 1990, Sol. Phys., 125, 219.

Skumanich, A., & Lites, B. W. 1987, ApJ 322, 473.

Tsuneta, S., *et al.* 1991, Sol. Phys., 136, 37.